AD 744465

DOCUMENT CONTROL DATA - R & D

(Security classification of title, body of abstract and indexing annotation must be entered when the overall report is classified)

1. ORIGINATING ACTIVITY (Corporate author)
Aerospace Medical Research Laboratory
Aerospace Medical Div, Air Force Systems Command
Wright-Patterson Air Force Base, Ohio 45 33

2a. REPORT SECURITY CLASSIFICATION
Unclassified

2b. GROUP
N/A

3. REPORT TITLE

THE BIOMECHANICS OF SPINAL AND HEAD IMPACT: PROBLEMS OF MATHEMATICAL SIMULATION.

4. DESCRIPTIVE NOTES (Type of report and inclusive dates)

5. AUTHOR(S) (First name, middle initial, last name)

Y. King Liu, Ph.D.

6. REPORT DATE	7a. TOTAL NO. OF PAGES	7b. NO. OF REFS
December 1971	~~35~~ 36	~~27~~ 27

8a. CONTRACT OR GRANT NO.	9a. ORIGINATOR'S REPORT NUMBER(S)
b. PROJECT NO. 7231	AMRL-TR-71-29 Paper No. 28.
c.	9b. OTHER REPORT NO(S) (Any other numbers that may be assigned this report)
d.	

10. DISTRIBUTION STATEMENT

Approved for public release; distribution unlimited

11. SUPPLEMENTARY NOTES	12. SPONSORING MILITARY ACTIVITY
	Aerospace Medical Research Laboratory Aerospace Medical Div, Air Force Systems Command, Wright-Patterson AFB, OH 45433

13. ABSTRACT

The Symposium on Biodynamics Models and Their Applications took place in Dayton, Ohio, on 26-28 October 1970 under the sponsorship of the National Academy of Sciences - National Research Council, Committee on Hearing, Bioacoustics, and Biomechanics; the National Aeronautics and Space Administration; and the Aerospace Medical Research Laboratory, Aerospace Medical Division, United States Air Force. Most technical areas discussed included application of biodynamic models for the establishment of environmental exposure limits, models for interpretation of animal, dummy, and operational experiments, mechanical characterization of living tissue and isolated organs, models to describe man's response to impact, blast, and acoustic energy, and performance in biodynamic environments.

DD FORM 1 NOV 68 1473

Security Classification

2

PAPER NO. 28

THE BIOMECHANICS OF SPINAL AND HEAD IMPACT: PROBLEMS OF MATHEMATICAL SIMULATION

Y. King Liu, Ph.D.
Assoc. Prof. of Biomechanics
Tulane University School of Medicine
New Orleans, Louisiana 70112

ABSTRACT

The present expository paper examines the various mathematical models proposed in impact studies in general and those in connection with spinal and head injuries in particular. First, the concept of injury tolerance surface is introduced. When a complete mapping of this surface is in hand, then the probability of injury due to any acceleration vector can be evaluated. After reviewing a typical single-degree-of-freedom model, a quadrature scheme, based on classical Fourier transform technique, is proposed for obtaining the pulse response from the experimentally determined mechanical impedance. The ignoring of the spatial mass distribution is shown to be the source of many difficulties in simple models. Typical results for the pilot-ejection problem where the spatial mass distribution is accounted for is then given. The determination of input parameters necessary to implement this class of models is also briefly described.

The second part of the paper begins with a review and critique of a promising one-dimensional continuum model of head injury by Hayashi[14]. Exact wave-propagation solutions were obtained for the intracranial pressure and container acceleration. When compared with the approximate solution given previously, both mathematical and physical reasons were advanced for the improvement of this model. The relatively small number of dimensionless parameters of the anticipated improved Hayashi model will make any future discussions of the cavitation theory very much easier. The survey of two- or three-dimensional models is divided into axisymmetric, rotational and nonaxisymmetric versions of fluid-filled spherical shells. A brief summary of the implications of the idealizations discussed above to other critical organs of the human body concludes the paper.

INTRODUCTION

In the course of daily living, a host of circumstances confront the human body such that a mechanical input is imposed on it. Many are accidental, e.g., athletic injuries, automobile and industrial accidents, while others are preplanned, e.g., ejection from high-speed aircraft, manned launchings and recoveries of aircraft and spaceships on water or land. In either case, the knowledge of the response, tolerance and control of the body is highly desirable, and in many situations, quite imperative. In terms of its response to externally applied forces, the body obeys the laws of mechanics. There is little doubt that this particular structure will be with us for a long time to come. Any understanding or knowledge gained with respect to its structural mechanics will have a continuing significance. The analogy that the skeletal (bone) system corresponds to the main structural members of machines is a plausible one. In that spirit, ligaments and tendons are then cables and tie-bars and muscles are sources of motive power. It is inappropriate to carry the analogy too far. Examples of physiological function which has rare counterparts in machines are: (1) The neuromusculature can shorten as much as 60% of its resting length due to active contraction and generally sustain loads several times more than its bony part. (2) Living bone can repair itself after fracture.

The basic modeling objectives are two-fold: (a) To propose the simplest mathematical description consistent with explaining the physical phenomenon. At the core of the mathematical description, there is the anatomical and/or physiological framework upon which the model rests and, on the other hand, the biomechanical data needed to implement the model. (b) To provide, through the model or its improvement, new insights or predict new phenomena, which serve to indicate where the measuring devices should be placed. The development of meaningful experiments should be guided by some theory, no matter how simple. The construction of a meaningful theory, on the other hand, requires the availability of experimental data and clinical observations. If data are not provided or found, there is always the danger that the theory will be based on how the body could or should respond rather than on how it does.

INJURY TOLERANCE SURFACES

The mathematical models of the human body subjected to accelerations depend on the direction of the acceleration vector. The applied accelerations range from steady-state oscillations to abrupt pulses. For the sake of uniformity in the discussion to follow, we shall follow the physiological acceleration coordinate (G) system recommended by the Committee on Acceleration of the AGARD Aerospace Medical Panel as reported by Gell[1].

The fundamental problem in acceleration injury is the construction of tolerance surfaces in the 3-G space with a suitable quantity as parameter. For abrupt pulses, the time of uniform acceleration exposure is an obvious candidate as a parameter. This point of view is easily illustrated in the G_x-G_z plane. Coincidentally, most of the current

available laboratory data on acceleration injury tolerance are in these directions of impact. In Figure 1 the data of Eiband[2] is replotted for a uniform acceleration duration of 0.05 secs. The axes intercepts correspond to the known tolerance data for $\pm G_z$. The straight dotted lines represent the easiest analytical construction of this tolerance curve and is in no way suggestive of reality. In fact, from the F4C aircraft data in which the ejection seat is inclined 14^o towards the +x axis, a second-degree hyperbola, shown as a solid curve might be much more appropriate. Tolerance data for combinations of accelerations are woefully lacking even for the plane and is nonexistent for the 3-G space. Many acceleration environments are indeed in this category, e.g., (1) winged-aircraft and automobile collisions are points in the G_x-G_y plane; (2) helicoptor crashes are points in the G_z-G_x-G_y space. This concept of the tolerance surface is adapted from the theory of yield surfaces (in the principal stress space) in elasticity and plasticity.

REVIEW OF SIMPLE LUMPED-PARAMETER MODELS

Given a typical impact situation, one can usually discern the following elements: mass, elasticity, dissipation and the nature of the applied impulse, which contribute to the dynamic response of the body. Assuming linearity of the elements, one can obtain the response of a damped dynamic system to a given acceleration (or force) input, a(t), as the solution of the well-known differential equation:

$$\ddot{x} + 2\delta\omega_o\dot{x} + \omega_o^2 x = a(t), \tag{1}$$

where ω_o is the natural frequency, δ is the damping ratio and x(t) is the relative displacement of the support with respect to the mass. The solution of equation (1) for an arbitrary a(t) is in the form of Duhamel's integral:

$$x = D \exp\{(-\delta + i\sqrt{1 - \delta^2})\omega_o t\} + \int a(\tau)h(t - \tau)d\tau, \tag{2}$$

where D is an arbitrary constant dependent on the initial conditions, $i = (-1)^{\frac{1}{2}}$, exp = e and h(t) is the indicial response, i.e., the response to a Dirac-delta input, of the system. For quiescent initial conditions, it has been shown by many investigators, e.g., von Gierke[3], Kornhauser[4], Payne[5], that the system response can be divided into approximately two regions at a critical pulse duration, t_c. For $t < t_c$, influence on the system occurs only in the pulse area, which is equal to the imposed velocity change. For $t > t_c$, the pulse shape is the important factor. If one were to assume that the elastic element always breaks at a given peak force level, the so-called equal tissue strain assumption, it is then possible to relate the damage or injury, through the system response, to the parameters of the input pulse. Typically, the result is a plot of the maximum applied acceleration, A_m, versus the duration of the pulse, t_1, on a log-log scale, as shown in Figure 2. In this tolerance graph, the "knee" represents the critical duration, t_c. To its left, the region is sensitive to velocity-change and to its right, the peak acceleration of the pulse.

An alternative to the above is the use of response to a sinusoidal input to predict system response under arbitrary pulse loading. Let the input be the real part of

$$\tilde{a}(t) = Ae^{i\omega t} \tag{3}$$

where A is a complex constant. The solution to (1) subjected to the input of (3) may be written as:

$$x = B \exp\{(-\delta + i\sqrt{1 - \delta^2}\omega_o)t\} + Ae^{i\omega t}/Z(\omega), \tag{4}$$

where B is a complex constant dependent on the initial conditions, $Z(\omega)$ is the characteristic impedance and

$$Z(\omega) = m(\omega_o^2 - \omega^2 + 2i\delta\omega_o\omega). \tag{5}$$

The reciprocal of (5), i.e., $H(\omega) = 1/Z(\omega)$, is the transfer function or frequency response function. For steady-state motion, the transfer function is the ratio of the output (displacement) to the input (sinusoidal excitation).

If one attempts to experimentally identify the transfer function, an immediate difficulty arises. Because the human body parts consist of distributed masses, generally no point can be picked where the displacements of the effective mass can be measured. Coermann[6] circumvented this difficulty by adopting the concept of mechanical impedance. Specifically, mechanical or driving point impedance is defined as the ratio of the transmitted force, F_{tr}, to the velocity, $\dot{x}$, of that point where the force is transmitted. It is equivalent to electrical impedance if one were to choose the force-current analogy. This concept of mechanical impedance is not identical to characteristic impedance, $Z(\omega)$, defined in (4). To avoid confusion, we denote mechanical impedance by $Y(\omega)$, which is easily shown to have the following form:

$$Y(\omega) = \frac{(1 + 2i\delta\omega/\omega_o)m\omega}{\{1 - (\omega/\omega_o)^2\} + 2i\delta\omega/\omega_o} \tag{6}$$

or

$$|Y(\omega)| = |F_{tr}|/|\dot{x}| = m\omega\left\{\frac{1 + (2\delta\omega/\omega_o)^2}{\left[1 - (\omega/\omega_o)^2\right]^2 + (2\delta\omega/\omega_o)^2}\right\}^{\frac{1}{2}} \tag{7}$$

The value of frequency ratio, $\omega/\omega_o = p$, at which the above equation attains its maximum is found by setting $dY/dp = 0$. It can be shown to occur at

$$p = \{4\delta^2 + (1 + 8\delta^2)^{\frac{1}{2}}\}/\{1 + 8\delta^2 - 16\delta^4\}\ . \tag{8}$$

Using the above model, Coermann[6] vibrated human volunteers, dummies and animals in the sitting and standing position from 1 to 20 hertz. From the experimentally obtained frequency ratio corresponding to the peak of the mechanical impedance curve, he determined the damping ratio, δ, with the help of (8).

An interesting question suggests itself at this point: given the frequency response or the mechanical impedance of a system, what can one say about its response to an arbitrary pulse? Define

$$\bar{a}(\omega) = (1/2\pi)\int_0^{\infty} a(t)e^{-i\omega t}dt \qquad (9)$$

as the Fourier Transform of a(t). Its inverse transform is:

$$a(t) = \int_{-\infty}^{+\infty} \bar{a}(\omega)e^{+i\omega t}d\omega \ . \qquad (10)$$

Implicit in the above definitions is that the conditions for the existence of such a transform pair are satisfied and that a(t) = 0 for t < 0. The above synthesis when superposed on (4) yields

$$x = B \exp\{(-\delta + i\sqrt{1 - \delta^2})\omega_o t\} + \int_{-\infty}^{+\infty} H(\omega)\bar{a}(\omega)e^{i\omega t}d\omega \ . \qquad (11)$$

In words, the pulse response of system (1) is the sum of the transient solution and the inverse Fourier transform of the product of the frequency response function, H(ω) and the frequency spectrum, $\bar{a}(\omega)$, of the pulse. To compute the displacement response of the effective mass to an arbitrary pulse based on frequency response data, one needs only to compare (5) and (6) and note that

$$Y(\omega) = m^2\omega\omega_o^2\{1 + 2i\delta(\omega/\omega_o)\}/Z(\omega) \ . \qquad (12)$$

Neglecting the transients, we get

$$x = \int_{-\infty}^{+\infty} \frac{Y(\omega)\bar{a}(\omega)e^{i\omega t}d\omega}{m^2\omega_o^2\omega\{1 + 2i\delta(\omega/\omega_o)\}} \ . \qquad (13)$$

For specific analytical forms of Y(ω) and $\bar{a}(\omega)$, it may be possible to obtain an analytical expression for x. In other instances, the integrand in (13) is so complicated that the evaluation of the integral is a matter of great difficulty. The true value of (13) in the present problem is to use the experimentally determined mechanical impedance, Y(ω) to yield information about its response to an arbitrary pulse. For these cases, recourse generally has to be made to numerical methods. To accomplish the complex integration in (13), a feasible approach is to resolve the complex function into separate functions of real and imaginary part and integrate each separately. Rewriting (13) as

$$x(t) = \int_{-\infty}^{+\infty} F(\omega)e^{i\omega t}d\omega, \qquad (13')$$

where F(ω) = A(ω) + iB(ω). It follows therefore, that

$$x(t) = a(t) + ib(t) = \{a^2(t) + b^2(t)\}^{\frac{1}{2}}e^{i\phi(t)} \ , \qquad (14)$$

where

$$a(t) = \int_{-\infty}^{+\infty}\{A(\omega)\cosh\omega t - B(\omega)\sinh\omega t\}d\omega$$

$$b(t) = \int_{-\infty}^{+\infty} \{A(\omega)\ \sinh\omega t + B(\omega)\ \cosh\omega t\}d\omega$$

$$\phi = \tan^{-1}(b/a)\ .$$

The practical difficulty lies in the frequency range to be swept. If the test data obtained is, say, from 0 - 200 hertz, then the Hobson's choice is to sweep from -200 to +200 hertz in evaluating (14). The numerical quadrature required can be achieved through any number of standard integration routines. The use of a hybrid analog-digital computer should also accomplish the task in one operation, i.e., from the data obtained to the final tolerance graph.

The massive experimental program mounted on behalf of the single-degree-of-freedom model served to identify some of the critical organ systems associated with a given force environment. The best understood case is the caudocephalad or $+G_z$ acceleration where the most critical organ is the spine and the mode of injury is, with few exceptions, compression fracture of the vertebral end-plates. Given this critical injury information, it is possible to refine the model analysis and/or identification of the model parameters. Liu[7] recently reviewed the modelling and experimental progress made for the spine in the dynamic environment with particular emphasis in the $+G_z$ orientation. A brief summary of his conclusions appear in the next section of this paper.

The critical organs and failure criterion for other orientations of impact are only partially defined. It is in these orientations where the relationships given by equations (2) and (13) are still needed pending additional work which will delineate the failure modes in the critical organs. As an example, consider the dynamics of the head-neck junction, which has major implications in brain injury due either to whiplash or a direct blow to the head. Initially, it can be viewed as a single degree of freedom rotational problem, i.e., the dependent variable in (1) is the angular displacement, Θ, of the head. The driving point impedance has been determined in detail by Hodgson et al.[8] Assuming a linear, single-degree-of-freedom system the parameters, δ and ω_o, can be identified from the impedance data and then the response to a pulse is found from (2). Alternately, if one were to compare the experimentally determined impedance data with the response as given in (4), the data will indicate its deviations from the simple model. These deviations can either be due to additional degrees of freedom in the system and/or nonlinear material properties or geometry.

MODELS CONSIDERING MASS DISTRIBUTION

Liu[7] recently gave a review and an assessment of the multi-degree-of-freedom, discrete-parameter and continuous-parameter models of the spine under inertial loading and their relationships to the simpler models proposed earlier. The essential points made in that paper were:

(1) Most of the inconsistencies of the simple models were due to ignoring the spatial mass distribution.

(2) The possible occurance of shock waves in a lightly damped nonlinear rod model of the spine is due to an accumulation of small effects.

The shock forms as a result of the steepening of the negatively sloped portion of the input pulse and not as a function of rapid rise time alone as has been suggested in the literature.

(3) That a lumped-parameter equivalent to a continuous segment is valid provided its length is much shorter than the shortest wavelength of interest. If one were to have an understanding of the spinal injury mechanism, the wavelength of interest is, at least, the thickness of the disc.

(4) The initial curvature and the eccentric center of mass of the trunk (anterior to the vertebral bodies) places the spine under complex loading even under normal conditions. For impact loading, the situation is greatly exaggerated.

(5) In order to implement either the multi-degree-of-freedom configuration model of Orne and Liu[9] or the distributed-parameter model of Moffatt[10], a large amount of biomechanical data is needed, e.g., the inertial-property distribution of the head, neck and trunk, the failure surface of the intervertebral joint under complex loading and the initial configurations of the pilot prior to ejection, etc. Liu et al.[11] recently obtained the inertial properties of a segmented cadaver trunk. Figures 3-5 summarized their results for the distribution of mass, the centers of mass and moments of inertia respectively.

(6) The predominance of anterior-lip and/or compression fractures in the lower thoracic vertebrae during pilot ejection are primarily attributable to the large negative moments there and only secondarily to the axial and shear forces. These summary results are shown in Figures 6-8. The solid curves are the results obtained by using the inertial data of Liu et al.[11] as input to the model by Orne and Liu[9] and the dotted curves were the corresponding results using assumed data. Figure 9 illustrates the time history of the configuration changes of the spine under these same loading conditions.

HEAD IMPACT MODELS

The special vulnerability of the head to injury as compared to other parts of the human body is evidenced by the fact that about 75% of the fatalities from all accidents are linked to craniocerebral trauma. The Proceedings of the Conference on Head Injury, edited by Caveness and Walker[12] summarized the spectrum of activities in connection with the problem up to 1966. Recently, Goldsmith[13] reviewed the more current work. It would be superfluous to cite these contributions once more except perhaps in illustrating some inconsistencies which have entered the modeling of intracranial pressure in head impact. The main discussion will deal with models which have entered the literature since 1966.

Mathematical models of the head have been divided in much the same fashion as the major hypotheses proposed to explain head injuries due to impact. One group, the rotational school, has contended that the rotational acceleration induced by impact causes high shear strains in the brain matter, rupturing cerebral blood vessels and tissue. The cavitation school, on the other hand, has claimed that there exist points within the brain where the reduced pressure is sufficient to rupture the capillary walls. The normal transmural pressure of these capillaries is a few mm Hg; however, due to the impact, the transmural pressure is

suddenly increased, bursting the capillary. Of course, when the pressure is reduced to near vapor pressure of the brain substance, cavitation should take place. The catastrophic collapse of the bubbles thus formed is another possible cause of brain damage.

ONE DIMENSIONAL CAVITATION MODEL

The most recent one-dimensional continuum model was given by T. Hayashi[14]. The system consists of a rigid but massless vessel (skull) containing elastic fluid (brain and cerebrospinal fluid). The vessel is attached to a linear spring k, which represents the composite elastic properties of the helmet, skull, hair and elasticity of the wall. Thus, the problem can be simplified to that of a fluid "rod" enclosed in a rigid vessel with an attached spring striking a rigid wall, see Figure 10. The governing nondimensional differential equation is:

$$u_{\tau\tau} + \xi_{\tau\tau} = \xi_{xx}, \tag{16}$$

where the subscript is used to denote partial differentiation with respect to the independent variables, x and τ. The associated initial and boundary conditions are respectively:

$$\zeta(x,0) = u(0) = 0;\ \zeta_\tau(x,0) = 0;\ u_\tau(0) = V \tag{17}$$

$$\zeta(0,\tau) = \zeta(1,\tau) = 0;\ u(\tau) = \lambda\{\zeta_x(0,\tau) - \zeta_x(1,\tau)\}\ . \tag{18}$$

In terms of the original quantities (with tilde $\sim$), the variables in (16)-(18) have been nondimensionalized as:

$$\begin{aligned} &\zeta = \tilde{\zeta}/\ell;\ u = \tilde{u}/\ell;\ x = \tilde{x}/\ell;\ \tau = c\tilde{\tau}/\ell \\ &c = (B/\rho)^{\frac{1}{2}};\ k_f = BA/\ell;\ \lambda = k_f/k;\ V = v_o/c, \end{aligned} \tag{19}$$

where $\tilde{\zeta}(\tilde{x},\tilde{\tau})$ is the displacement of the fluid at location $\tilde{x}$ relative to the vessel, A is the area, ℓ is the length, $\tilde{\tau}$ is the time, $\tilde{u}$ is the absolute rigid-body displacement of the vessel, v_o = velocity of the vessel just prior to impact; B is the bulk modulus; ρ is the density; $c = (B/\rho)^{\frac{1}{2}}$ is the wave speed and k_f is the stiffness of the fluid. Hayashi[14] utilized a separation of variables technique to obtain an infinite series solution for the vessel displacement and the fluid pressure in the original variables, i.e., $\tilde{u}$ and $\tilde{\zeta}_{\tilde{x}}$. In terms of the dimensionless variables given in (19), his solutions can be written as:

$$u(\tau) = 2V \sum_{n=1}^{\infty} \frac{\sin(2\omega_n)}{(2\omega_n)\{2\omega_n + \sin(2\omega_n)\}} \sin(2\omega_n\tau) \tag{20}$$

and

$$-P(x,\tau) = -\frac{\zeta_x(x,\tau)}{B}$$

$$= 4V \sum_{n=1}^{\infty} \frac{\sin(\omega_n)}{2\omega_n + \sin(2\omega_n)} \sin\{\omega_n(1-2x)\} \sin(2\omega_n\tau), \tag{21}$$

where ω_n are the n roots of the characteristic equation:

$$\omega \tan\omega = \frac{1}{4\lambda} \tag{22}$$

The roots of (22) are partially tabulated in the National Bureau of Standards Handbyok of Mathematical Functions (edited by Abramowitz and Stegun). Any attempt to perform computations using (20) - (22), however, would show that these infinite series solutions are slowly convergent, if at all, especially for small values of time. In short, while (20) and (21) are nominally "exact" solutions, they are useless in computing numerical results. If, in addition, certain approximations are made in order to make (20) - (22) more pliable, the errors are then compounded as will be shown presently by the exact closed form solution obtained by the author.

Taking the Laplace transform of Equations (16) to (18) yields

$$\overline{\zeta}(x,p) = -\frac{V\{\cosh px - \tanh(p/2)\ \sinh px - 1\}}{p^2\{1 + 2\lambda p\ \tanh(p/2)\}} \tag{23}$$

and

$$\overline{u}(p) = \frac{2\lambda V\ \tanh(p/2)}{p\{1 + 2\lambda p\ \tanh(p/2)\}} \cdot \tag{24}$$

The pressure in the fluid is found from the inversion of:

$$\overline{P}(x,p) = -\overline{\zeta}_x(x,p) = \frac{V\{\sinh px - \tanh(p/2)\ \cosh px\}}{p\{1 + 2\lambda p\ \tanh(p/2)\}} \quad . \tag{25}$$

The poles of (25) are the characteristic roots of (22). Using the standard contour inversion integral and summing the residues will yield identical results as those shown in (20) and (21). We are back in the same quandary! Under these circumstances, instead of dealing with the entire function, one circumvents the problem by dealing with its expansion, see Carslaw and Jaeger[15]. Expanding the hyperbolic functions in terms of exponentials, we write (25) as:

$$\overline{P}(x,p) = \frac{-V\{e^{-px} - e^{-p(1-x)}\}}{p(1+2\lambda p)\{1+\varepsilon(p)e^{-p}\}} , \tag{26}$$

where

$$\varepsilon(p) = \frac{2}{1 + 2\lambda p} - 1 \tag{27}$$

Using the binomial theorem, we get

$$\left\{1 + \varepsilon(p)e^{-p}\right\}^{-1} = 1 + \sum_{n=1}^{\infty} (-1)^n \varepsilon^n(p) e^{-np} \quad . \tag{28}$$

Observe that

$$(-1)^n\varepsilon^n(p) = \left\{1 - \frac{2}{1+2\lambda p}\right\}^n = 1 + \sum_{\nu=1}^{n} (-1)^{\nu} \binom{n}{\nu} \lambda^{-\nu} \left(p+\frac{1}{2\lambda}\right)^{-\nu} \tag{29}$$

where $\binom{n}{\nu} = \frac{n!}{\nu!(n-\nu)!}$ are the binomial coefficients.

In view of (28) and (29), (25) becomes

$$\bar{P}(x,p) = \frac{-V}{p(1+2\lambda p)}\left\{\left[e^{-px}-e^{-p(1-x)}\right] + \sum_{n=1}^{\infty} e^{-p(n+x)} - \sum_{n=1}^{\infty} e^{-p(n+1-x)}\right.$$

$$\left. + \sum_{n=1}^{\infty}\sum_{\nu=1}^{n}(-1)^{\nu}\binom{n}{\nu}\lambda^{-\nu}\left(p+\frac{1}{2\lambda}\right)^{-\nu}\left[e^{-p(n+x)}-e^{-p(n+1-x)}\right]\right\} \tag{30}$$

The inverse of $1/p(p+\frac{1}{2\lambda})^{\nu+1}$ is

$$\frac{1}{2\pi i}\int_{\gamma-i\infty}^{\gamma+i\infty}\left[e^{p\tau}/p(p+\frac{1}{2\lambda})^{\nu+1}\right]dp = (2\lambda)^{\nu+1}\left[1-e^{-\tau/2\lambda}\sum_{\mu=0}^{\nu}\frac{\tau^{\mu}}{(2\lambda)^{\mu}\mu!}\right] \tag{31}$$

Taking advantage of the shifting theorem, the <u>exact</u> solution to the problem posed by (16) - (18) is:

$$-\frac{P(x,\tau)}{V} = \left[1-e^{-(\tau-x)/2\lambda}\right]H(\tau-x) - \left[1-e^{-(\tau-1+x)/2\lambda}\right]H(\tau-1+x)$$

$$+\sum_{n=1}^{\infty}\left[1-e^{-(\tau-n-x)/2\lambda}\right]H(\tau-n-x) - \sum_{n=1}^{\infty}\left[1-e^{-(\tau-n-1+x)/2\lambda}\right]H(\tau-n-1+x)$$

$$+\sum_{n=1}^{\infty}\sum_{\nu=1}^{n}(-1)^{\nu}\binom{n}{\nu}\frac{1}{\lambda^{\nu}(2\lambda)^{-\nu}}\left\{\left[1-e^{-(\tau-n-x)/2\lambda}\sum_{\mu=0}^{\nu}\frac{(\tau-n-x)^{\mu}}{\mu!(2\lambda)^{\mu}}\right]H(\tau-n-x)\right.$$

$$\left.-\left[1-e^{-(\tau-n-1+x)/2\lambda}\sum_{\mu=0}^{\nu}\frac{(\tau-n-1+x)^{\mu}}{\mu!(2\lambda)^{\mu}}\right]H(\tau-n-1+x)\right\} \tag{32}$$

Where H(t) is the Heaviside function, i.e., it is zero when $t < 0$ and unity when $t > 0$.

We note that (32) is an odd function about $x = \frac{1}{2}$, i.e.,

$$P(x,\tau) = -P(1-x,\tau) \tag{33}$$

and in particular

$$P(0,\tau) = -P(1,\tau). \tag{33'}$$

For $x = \frac{1}{2}$, $P(\frac{1}{2},\tau) = -P(\frac{1}{2},\tau)$, which is possible if and only if $P(\frac{1}{2},\tau) \equiv 0$. Equation (33) states that the pressure at the center is always zero and the pressure variations in time are equal, except for sign, on either side of the center. Further, the solution (32) is valid only prior to rebound which occurs when $F = k\ddot{u} \geq 0$. In view of (18) and (33'), the rebound condition is

equivalently

$$-P(0,\tau) \geq 0, \tag{34}$$

i.e., when the system returns to the initial position of the container prior to impact. Due to the nature of the Heaviside function, for a given x and τ, only a finite number of terms are needed from (32) to perform the numerical calculations, attesting to its simplicity as well as exactness. For up to 2 wave-transit times even hand calculations would suffice.

The displacement can be found immediately from the boundary condition (18), i.e.,

$$u(\tau) = \lambda\{\zeta_x(0,\tau) - \zeta_x(1,\tau)\} = -2\lambda P(0,\tau), \tag{35}$$

where use was made of $P(x,\tau) = -\zeta_x(x,\tau)$ and $P(0,\tau) = -P(1,\tau)$. The differentiation in the τ domain corresponds to multiplication by p since the initial displacement is zero, hence

$$pu(p) = 2\lambda V \tanh(p/2)\{1 + 2\lambda p \tanh(p/2)\}^{-1}. \tag{36}$$

To check that the initial velocity is satisfied, we note

$$u_\tau(0) = \lim_{p\to\infty} p^2\bar{u}(p) = \lim_{p\to\infty}\{2\lambda V p \tanh(p/2)\left[1+2\lambda p \tanh(p/2)\right]^{-1}\}$$

$$= \lim_{p\to\infty} \frac{2\lambda V \tanh(p/2)}{1/p + 2\lambda \tanh(p/2)} = V. \tag{37}$$

The acceleration is, therefore, the inverse transform of

$$\bar{a}(p) = p^2\bar{u}(p) - u_\tau(0) = \frac{V\{2\lambda p \tanh(p/2) - 1\}}{1 + 2\lambda p \tanh(p/2)} \tag{38}$$

Through an expansion and inversion procedure similar to (26)-(29), we obtain

$$\frac{-2\lambda a(\tau)}{V} = e^{-\tau/2\lambda}H(\tau) + 2\sum_{n=1}^{\infty} e^{-(\tau-n)/2\lambda}H(\tau-n)$$

$$+ \sum_{n=1}^{\infty}\sum_{\nu=1}^{n} (-1)^\nu \binom{n}{\nu} \frac{1}{\lambda^\nu \nu!}\left[(\tau-n)e^{-(\tau-n)/2\lambda}H(\tau-n)\right.$$

$$\left. - (\tau-n-1)e^{-(\tau-n-1)/2\lambda}H(\tau-n-1)\right]. \tag{39}$$

Equations (39) and (32) constitute the exact principal results of the model. The corresponding Hayashi approximate results are found from (20), (21) and (22) by the substitution of $\omega_1 \doteq 1/2\lambda^{\frac{1}{2}}$ into the infinite series truncated after one term, i.e.,

$$-\frac{2\lambda a}{V} = 2\lambda^{\frac{1}{2}} \sin(\tau/\lambda^{\frac{1}{2}}) \qquad (20')$$

$$-\frac{P(x,\tau)}{V} = \frac{(1-2x)}{2\lambda^{\frac{1}{2}}} \sin(\tau/\lambda^{\frac{1}{2}}) \qquad (21')$$

Figure 11 is a plot comparing the acceleration of the container as obtained by equation (39) and (20') for different values of stiffness ratio λ. Whereas the exact wave propagation solution has a discontinuous jump at $\tau = 0$ and "jumps" at $\tau = 1,2,\ldots$, the points of wave reflection, in contrast, the Hayashi approximation is a sine wave. The discontinuous jumps shown in Figure 11 have major implications for the infinite series solutions such as (20) and (21). Would the addition of more terms from (21) improve the acceleration result? It is well-known, however, that the partial sums $S_m(x)$ of a Fourier series for a periodic function f cannot approach f(x) uniformly over an interval that contains a point where f is discontinuous. The nature of the deviation of $S_m(x)$ from f(x) on such intervals is known as Gibb's phenomenon, see Carslaw[17]. The pathological nature of the exact acceleration solution was due to the absence of the container mass, which is to be regarded as a weak solution in the sense of Courant and Hilbert[18].

For the pressure results, two sets of graphical data are of interest: (a) the pressure field variation at given times, and (b) the pressure-time variation at a given location, x. In Figure 12 is shown the dimensionless contrecoup ($x = 0$) pressure as a function of τ. When the contrecoup pressure reaches zero, the solution (32) is no longer valid because of the rebound condition (34). Note that the softer the impact, (increasing λ) the longer the contact duration, τ_c, e.g., $\lambda = 1$, $\tau_c \simeq 3.275$, whereas $\lambda = 0.1$, $\tau_c \simeq 1.34$. For very soft impacts, $\lambda >> 1$, the pressure wave would have traversed the fluid length many times during the time the vessel takes to return to its original position, i.e., just prior to loss of contact. Also shown in Figure 12 is a comparison of the exact wave-propagation solution with the Hayashi approximate solution for various λ. We note with interest that for $\lambda = 10$ the two results are indistinguishable and that for $\lambda = 1$, the approximation is still quite good. It would appear that in all practical cases of interest, the approximate pressure solution would suffice.

Figures 13 and 14 are plots of the pressure fields for time increments, $\Delta\tau = 0.1$ and $\lambda = 1$ and $\lambda = 10$. Up to $\tau = 0.5$, the pressure distribution reflects the wave-propagation nature of the problem. After traversal is completed, i.e., $\tau > 0.5$, the distribution deviates somewhat from the usual experimental observation that the pressure field is linear for any given τ, e.g., Roberts et al.[16]

Figure 15 replots the pressure-time variation at a given point for $\lambda = 0.1$, 1 and 10. The approach to zero pressure at the center of the container is quite abrupt when one considers the amount of pressure fluctuations still present at $x = 0.4$.

An overview of Figures 11 - 15 would indicate that the Hayashi approximation for the pressure is excellent for $\lambda \geq 10$. To correlate the pressure distribution, however, to a "maximum acceleration", which is due entirely to an approximation, is not self-consistent. The remarkable agreement with experimental data given by Hayashi, reproduced here as Figure 16, should be considered fortuitious at this time. On the other hand, in spite of its analytical pathology, the concept of an acceleration beginning at zero and in phase with the fluid pressure as postulated by Hayashi has intuitive and physical appeal. The weaknesses of the model lie obviously in neglecting the container mass and possibly dissipation. Typically, one can add a damper, c, in parallel with the spring, k, and include the vessel mass, i.e., the boundary condition (18) takes the dimensionless form:

$$u + \eta u_\tau + \lambda\mu u_{\tau\tau} = \lambda\{\zeta_x(0,\tau) - \zeta_x(1,\tau)\} \quad , \tag{40}$$

where μ is the container to fluid mass ratio and η is a damping parameter. In a preliminary study, the author has shown that the container acceleration is indeed smoother than the "jumps" indicated in Figure 15, e.g., the acceleration has a finite rise time from zero. When these improvements are completed, the model first proposed by Hayashi might indeed still make the discussion of the cavitation model very much easier because of the relatively small number of dimensionless parameters present.

TWO DIMENSIONAL MODELS

The use of a fluid-filled rigid spherical shell under impact as a model of craniocerebral trauma began with Anzelius[19] and Güttinger[20]. Phenomenologically, this model is not very different from the one-dimensional one just discussed. Because of the rigid assumption, a blow at one point (coup) on the sphere is immediately transmitted to the diametrically opposite pole (contrecoup). Every point on the shell begins to transmit energy at the instant of impact. Goldsmith[13] suggested the obvious necessity of modelling the skull as an elastic shell. Engin and Liu[21] justified the use of a fluid-filled elastic spherical shell as a model for head injury based on neuroanatomical and analytical considerations. They obtained the frequency spectrum for the axisymmetric free vibration of the fluid-solid ensemble and compared the results for the cases of steel and water and skull and water. The axisymmetric response of a thin, elastic, homogeneous and completely closed spherical shell filled with an inviscid and irrotational fluid subjected to a radial impulse was obtained by Engin[22]. The point of view taken is that of a spherical fluid region constrained by very complicated boundary conditions consisting of the two shell differential equations (including both bending and membrane effects) and the continuity of the normal velocity at the fluid-solid interface. Mathematically, this is expressed by satisfying the wave equation in

The pathological nature of these solutions were a consequence of the mathematical formulation of the problem, Wave propagation phenomena are represented by solutions of hyperbolic differential equations with prescribed initial and boundary data. If the given data is discontinuous (e.g., wave motion initiated by an impulse: $u_\tau(0) = V$) the solution is also discontinuous. The function $f(x + \tau) + g(x - \tau)$ is a genuine solution of the wave equation provided f and g are twice differentiable. Otherwise, the function ought to be regarded as a "solution in the general sense" or a weak solution, see Courant and Hilbert.[18]

Because of the inherent weaknesses of the above one-dimensional model due to both the mathematics and obvious geometrical restraints, further improvement of this model appears superfluous. Typically, if one were to add a damping element in parallel or in series with the spring and include the inertia of the container, i.e., boundary condition (18) takes the form:

$$u + \eta u_\tau + \mu u_{\tau\tau} = \lambda\{\zeta_x(0,\tau) - \zeta_x(1,\tau)\} , \qquad (40)$$

where η and μ are the dimensionless damping and inertial parameters respectively. A similar analysis as given earlier would yield the presence of a Dirac-delta function in the pressure field, which is physically untenable.

It is indeed regrettable that the one-dimensional continuum model proposed by Hayashi is beset by these mathematical difficulties. The model has the advantage of simplicity. If it had satisfied the test of self-consistency, its small number of dimensionless parameters would have made discussions of the cavitation model very much easier.

TWO DIMENSIONAL MODELS

The use of a fluid-filled rigid spherical shell under impact as a model of craniocerebral trauma began with Anzelius[19] and Güttinger[20]. Phenomenologically, this model is not very different from the one-dimensional one just discussed. Because of the rigid assumption, a blow at one point (coup) on the sphere is immediately transmitted to the diametrically opposite pole (contrecoup). Every point on the shell begins to transmit energy at the instant of impact. Goldsmith[13] suggested the obvious necessity of modelling the skull as an elastic shell. Engin and Liu[21] justified the use of a fluid-filled elastic spherical shell as a model for head injury based on neuroanatomical and analytical considerations. They obtained the frequency spectrum for the axisymmetric free vibration of the fluid-solid ensemble and compared the results for the cases of steel and water and skull and water. The axisymmetric response of a thin, elastic, homogeneous and completely closed spherical shell filled with an inviscid and irrotational fluid subjected to a radial impulse was obtained by Engin[22]. The point of view taken is that of a spherical fluid region constrained by very complicated boundary conditions consisting of the two shell differential equations (including both bending and membrane effects) and the continuity of the normal velocity at the fluid-solid interface. Mathematically, this is expressed by satisfying the wave equation in

axisymmetrical spherical coordinates for the fluid exactly, i.e., the velocity potential of the fluid in the Laplace-transformed variable is expanded in an infinite series of its characteristic functions. On the other hand, the shell equations are expanded in terms of Legendre and associated Legendre polynomials, which are the characteristic functions for the in-vacuo shell differential equations. The ensuing infinite series solutions have this inherent error of truncation.

The above comments have a familiar ring and one might immediately and legitimately question whether or not the solutions thus obtained fall into the same quagmire as the infinite-series solution in the Hayashi model. There exists no exact solution, such as the wave propagation result, to settle the question definitively. In Engin's solution, the intracranial pressure required the evaluation of 420 residues in order to achieve convergence in the sense of Cauchy. There is every physical reason to believe however, that these solutions will not contain discontinuous jumps. By comparison with the one-dimensional model, the fluid-solid model has the following advantages in this regard:

(a) The container (shell) is elastic and hence it takes a finite time for the stress waves to travel from coup to contrecoup. The instantaneous transmission of pressure waves due to the assumption of rigidity of the container is one contribution to the jump phenomena discussed earlier and also observed in the solutions due to Güttinger[20].

(b) The load on the shell is spread over a finite area (a polar cap) while in the one dimensional model it is confined to a point, a physically untenable state.

(c) The obvious geometrical advantage in being able to spread the pressure variation as a function of the polar angle, radius and time.

The results of Engin confirmed that most likely locations of skull fracture are away from the impact polar cap. Specifically, for a blow of uniform pressure over a 15^{o} cone angle, the location of high stresses on the skull are immediately below the impact area and in a ring about 45^{o} away from the polar axis. The second interesting result is the pressure distribution in the brain during a closed-head trauma. If one assumes, for the moment, that injury is associated with negative pressure, then the possibility of intermediate coup, i.e., high negative pressures away from the contrecoup point, has been predicted by the model. Liu and Nelson[23] have extended Engin's result and compared the differences in pressure-wave propagation between a Dirac-delta type impulse to a more realistic finite time pulse. Because of the complexity of the wave interaction phenomena, they have produced a "cartoon" type movie showing the progress of the "isobars" in the brain. For the Dirac-delta time function, the frames corresponding to contrecoup and intermediate coup are shown in Figures 17 and 18. In these figures, the symbols +, 0, 1, 2, 3, 4 and 5 represent intervals of increasing negative nondimensional pressure while the symbols -, =, A, B, C, D, E, and F denote increasing positive nondimensional pressures. The dimensionless pressure, p_1 and time τ are related to the physical quantities as follows:

$$p_1 = \rho_s(1 - \nu^2)p/E\rho_f \ , \tag{41}$$

$$\tau = c_s t/a, \tag{42}$$

where ρ_s and ρ_f are the densities of the skull and fluid respectively, E and ν are the Young's modulus and Poisson's ratio of the shell and p is the magnitude of the externally applied uniform pressure, c_s is the wave speed in the shell and is equal to $\{E/\rho_s(1-\nu^2)\}^{\frac{1}{2}}$, a is the radius of the shell and t, the time.

We note from Figures 17 and 18, the following:

a) There exists a "ringing" motion in the fluid, i.e., the alternating positive and negative pressures in each frame.

b) The so-called contrecoup negative pressure is low in magnitude (grade 1) but diffuse over a fairly large area.

c) The intermediate-coup negative pressure is high in magnitude (grade 5) but extremely well-focused.

The response of the fluid-solid interaction system to a more realistic finite time-varying pulse is obtained by convolution. Using the same spatial distribution as Engin, but instead of the Dirac-delta function, we use

$$T(t) = \exp\ (-4.73 \times 10^{-6}t^2)\ \sin(\pi \times 10^{-3}t) \tag{43}$$

The pressure response of the system is similar except that the "ringing" is more pronounced and the contrecoup area less diffused. It was evident from an examination of the frames that the damage criterion for any given location must incorporate the following factor: the time spent beyond a critical negative pressure. Physiological considerations collaborate the above argument. The capillaries will not burst even for a large transmural pressure if the negative pressure is present for only a very short time. Finite time is required for the blood to enlarge the capillary walls to the point of rupture. On the other hand, a small transmural pressure acting over a relatively long period of time can damage the vessel. From simple strength of material, the static hoop stress, σ, for a thin-walled tube is

$$\sigma = \Delta pd/2h, \tag{44}$$

where Δp is the transmural pressure, h/d is the wall thickness to diameter ratio. According to Burton[24], h/d is about 1/8 for a true capillary. Its thickness is practically a single layer of endothelial lining cells. Very little force is required to deform these cells and they are believed to play a very minor role in the total elasticity. Without going into the role of the surrounding tissue, it suffices to note that equation (44) is the basis of those who claim that negative pressure is the damage criterion. Liu and Nelson[23] postulated the following Cummulative Damage Criterion for closed-head brain injuries: The severity of the brain injury at a given location is proportional to the averaged time spent there beyond a critical negative pressure, p*. This criterion is illustrated in Figure 19. The negative pressure less than p*, at location x_o, is divided into equal time steps Δt apart. Let $p_1(x_o,\Delta t_2)$, $p_2(x_o,\Delta t_2)$, - - - -, $p_i(x_o,\Delta t_i)$ be the lengths of a series of chords representing the discrete pressures at the beginning of its Δt_i, then

the time-averaged pressure $\bar{p}(x_o,\bar{t})$ is given analytically by:

$$\bar{p}(x_o,\bar{t}) = \sum_{i=1}^{n} p_i(x_o,\Delta t_i)H(p^* - p_i)/\sum_{i=1}^{n}\Delta t_i, \qquad (45)$$

where $H(p^* - p_i)$ is the Heaviside function, i.e., it is zero if $p^* < p_i$ and is unity of $p^* > p_i$. The maximum value of $\bar{p}(x_o,\bar{t})$ is assigned a grade of 5 and a decreasing linear scale is used thereafter for the lower pressures. The computations were terminated at the end of the applied pulse. By the Cumulative Damage Criterion, there appears two foci of intermediate-coup due essentially to the wave propagation and interaction phenomena and con' recoup because of the induced accelerational difference between the shell a d the fluid.

Th situation appears paradoxical at this point. As the elasticity of the shell is taken into account, the analysis seems to deviate more and more from the comfortable notion of a linear pressure distribution reported by the experimentalists, see, for example, the works of Lingren[25], Unterharnscheidt and Sellier[26], and Roberts et al.[16]. The situation is not an unfamiliar one. The experimentalists made measurements without a theoretical model, or at best, the model was constructed from the data a posteriori without much regard for the fundamental requirements of the boundary-value problem. On the other hand, the analysts have not been concerned with the experimental evidence of the suitability of his basic assumptions or if he has, found the experimental situation too difficult to formulate in analytical terms. Hopefully, this disagreement will be resolved as additional experimental and analytical work presently in progress is published.

Recently, Lee and Advani[27] partially extended the model of Engin and Liu[21] to include transverse shear and rotational inertia in the shell approximation. The net effect of this improvement is to include wavelengths of the order of the thickness of the shell. The qualitative differences between their result and Engin's were negligible for radial displacement and fibre stresses. Unfortunately, the boundary-value problem associated with the fluid pressure determination was not solved. It is precisely in the fluid, however, where the "high frequency" effects would be most manifest.

Except for the extremely unusual case in which the blow is delivered such that its resultant force passes through the center of mass of the head, the head will experience both a translation and rotation. In the case of a whiplash-type of injury, one also expects both motions to occur. To assess the relative contributions of each of these proposed damage mechanisms to head trauma, Chan[28] is presently investigating the non-axisymmetric response of a fluid-filled spherical shell. The fluid is considered inviscid and irrotational and an "exact" six mode shell theory is used. The implications of the latter is that the analysis will be valid for a thick shell, i.e., its radius to wall-thickness is between 4 and 10. The loading consists of an axisymmetric pulse perpendicular to the surface and a traction tangential to it.

ROTATIONAL IMPACT MODELS

Because of the very small shear modulus of the brain compared with its bulk modulus, Holbourn[29] was the first to postulate the possibility of brain damage due to rotational acceleration alone. Von Gierke[3] gave, for soft tissue, a value for volume compressibility of 2.6×10^{10} dyne/cm^2 as compared to a shear elasticity of 2.5×10^4 dyne/cm^2. He further noted that when soft tissue is subjected to a blow most of the energy spreads through the tissue in the form of shear waves and not of compression waves. Only very rapid blows produced compression waves of appreciable magnitude in tissue. The implications for energy transmission in the soft brain tissue is obvious. Engin and Wang[30] gave a theoretical analysis of the driving point impedance test for a continuum model of the brain. Relationships were derived from which some of the viscoelastic parameters can be determined from the experimental data.

Holbourn's observation has been pursued further by Ommaya et al.[31] and Unterharnscheidt and Higgins[32]. The mathematical models used were the single degree of freedom rotational version of equation (1) with the angular head displacement θ as the dependent variable and the angular acceleration as input. The motion of the head is modelled as a rigid body constrained by a torsional spring. The failure criterion is a clinical indicator of concussion. The resultant data is correlated with the parameters of the input pulse in a form similar to Figure 3.

Martinez and Garcia[33] used a three-degrees-of-freedom nonlinear model to describe the whiplash phenomena. The head is represented by a mass and the resistance of the neck to rotation and shear are represented by torsional and cantilevered springs respectively. Roberts et al.[34] divided the head into two rigid-body compartments: the skull and the brain. A torsional spring placed at the center of the head simulates the resistance of the brain to rotation relative to the skull. The resistance to linear displacement is simulated by linear spring connecting the brain to the skull. A parametric study was made using many assumed input system constants. Hayashi[35] noted that for very short-duration rotational impact, the severest shear deformation is induced in the boundary layer near the inner surface of the skull. From this observation, he constructed a model consisting of two concentric cylinders, which are connected elastically in shear by the brain material. The cylinders are assumed to be rigid bodies: the outer shell representing the skull and the inner one the essentially undeformed portion of the brain. Using estimated input data and a data point on the tolerance curve due to Ommaya et al.[31], he obtained through his analysis a tolerance relationship:

$$\ddot{\theta}^* t_D^2 = 2.52, \tag{46}$$

where $\ddot{\theta}^*$ is the critical or maximum input angular acceleration and t_D is the impact duration.

The first two-dimensional continuum model for torsional impact to the head was proposed by Lee and Advani[36]. The model is a linear elastic sphere subjected to a step angular acceleration about a diametrical

axis. The displacement is prescribed to be zero at the surface of the sphere. The results are expressions for the dynamic torsional displacement and shear stress. The maximum torsional displacement occurs approximately at normalized radius r = 0.42. There is a rapid buildup of shear stresses at the surface of the sphere. If the time for a shear wave to travel from the surface to the center is normalized to unity, then for nondimensional time of less than one ($t < 1$), the shear stress decreases with radius, i.e., reaching zero at the appropriate point. Of course nothing happens prior to the arrival of the stress wave. For $t > 1$, the stress distribution is almost linear with respect to the zero at the origin. In addition, the linear viscoelastic response of the sphere is studied by using a superposition principle. The numerical results for a Maxwell fluid model indicate an almost logarithmic attenuation of shear stress with respect to the dimensionless radius.

OTHER CRITICAL ORGANS AND CONCLUDING REMARKS

While attention has been focused on the situation where the spine and head are the critical organs, all the perspectives gained hopefully have implications in other impact situations. For instance, the critical organ in human tolerance to blast exposure is most probably the lung. Sass[37] has contended that the lung is the most susceptible organ to injury because of its low density and elasticity and non-rigid envelope, while the brain is the least vulnerable because of its essential incompressibility and rigid enclosure. Experimental and theoretical support for this contention has not been conclusive. Failure criterion in materials, whether biological or not, is given in terms of stresses, which are then related to the strains through constitutive equations. The strain-displacement relationships provide the final link to the relative motion of the body tissues. Unless and until the intermediate relationships are known, excessive displacement or rate of displacement can not by itself be a criterion of injury susceptibility. A good illustrative example is the predominance of compression fracture of the vertebral end-plates and anterior lip fractures in caudocephalad acceleration. Without doubt, in this mode of acceleration, relatively large displacements of the lungs and diaphragm do take place as evidenced by some occurrances of lung and visceral injury in pilot ejection. Of course, these critical organs can be analyzed in a similar way as the spine and head. The question is always one of priority.

A synopsis of the exposure limits for human tolerance to blast will reveal a similar hierarchy of idealizations in the modelling process. The initial linearized model due to von Gierke[3] involved the concept of equal strain in lung tissue. Tolerance curves plotting the maximum overpressure versus the duration of exposure were given. An improved model due to Holladay and Bowen[37] accounted for the nonlinear effects due to large amplitude pressure waves and severe compression of the lung volume. Further refinement of the model probably lies in the continuum notion that there exists a wave transmission through the skin, the neuromusculature, the thoracic cage and the lung tissue while simultaneously the blast wave works its way down the bronchial tree. The possible interaction of these two waves of differing speeds might be reflected in the intrapulmonary pressure measurements.

REFERENCES

(1) Gell, C. F., "Table of equivalents for acceleration terminology recommended by the Committee on Acceleration of the AGARD Aerospace Medical Panel". Aerospace Med. 32:1109-1111, 1961.

(2) Eiband, A. M., "Human tolerance to rapidly applied accelerations: a summary of literature". NASA Memo 5-19-59E. National Aeronautics and Space Administration, Washington, D. C., 1959.

(3) von Gierke, H. E., "Biodynamic response of the human body", Applied Mechanics Reviews, 17, pp. 961-968, 1964.

(4) Kornhauser, M., Structural Effects of Impact, Spartan, Cleaver-Baltimore, 1962.

(5) Payne, P. R., Personnel Restraint and Support System Dynamics, TR-65-12F, Aerospace Med. Research Labs., October, 1965.

(6) Coermann, R. R., "Comparison of the dynamic characteristics of dummies, animals and man" Proc. National Academy of Sciences Symposium on Impact Acceleration Stress, Brooks AFB, San Antonio, Texas, November, 1961.

(7) Liu, Y. King, "Distributed-parameter dynamic models of the spine". Proc. Workshop on Bioengineering Approaches to the Problems of the Spine, Bethesda, Maryland, September, 1970.

(8) Hodgson, V. R., Gurdijian, E. S. and Thomas, L. M., "The determination of response characteristics of the head with emphasis on mechanical impedance techniques". 11th Stapp Car Crash Conference, 125-138, 1967.

(9) Orne, D. and Liu, Y. King, "A mathematical model of spinal response to impact". J. Biomechanics, 4, No. 4, October, 1970. Also as A.S.M.E. preprint No. 70-BHF-1.

(10) Moffatt, C. A., Private communication, 1970.

(11) Liu, Y. King, Laborde, J. M. and Van Buskirk, W., "Inertial properties of a segmented cadaver trunk: their implications in acceleration injuries," submitted to Aerospace Medicine for publication.

(12) Caveness, W. F. and Walker, A. E., eds., Proc. of Head Injury Conference, Lippincott, 1966, University of Chicago.

(13) Goldsmith, W. "Biomechanics of Head Injury" Symp. on the Foundations and Objectives of Biomechanics, University of California-San Diego, July, 1970.

(14) Hayashi, T., "Study of intracranial pressure caused by head impact," Jour. Faculty of Engr. Univ. of Tokyo, 30, 59. 1969.

(15) Carslaw, H. S. and Jaeger, J. C., Operational Methods in Applied Mathematics, 2nd Ed. Oxford University Press, 1948. Also as Dover paperback, 1963.

(16) Roberts, V., Hodgson, V., and Thomas, L. M. "Fluid pressure gradients caused by impact to the human skull, Biomechanics Monograph ASME: 223, 1967.

(17) Carslaw, H. S., Theory of Fourier's Series and Integrals, Dover, paperback in 1963.

(18) Courant, R. and Hilbert, D., Methods of Mathematical Physics, Vol. II: 486 Interscience-Wiley, 1962.

(19) Anzelius, A., "The effect of an impact on a spherical liquid mass." Acta. Path. Microbiol. Scand. Supplement 48, 1943.

(20) GÜttinger, W. "Der Stosseffect auf eine Flüssigkeitskugel als Grundlage einer Physikalischen Theorie der Entstehung von Gehirnverletzungen," Zeit. f. Naturforschung. 5, 622, 1950.

(21) Engin, A. E. and Liu, Y. King, "Axisymmetric response of a fluid-filled spherical shell in free vibrations" J. of Biomechanics, Vol. 3, No. 1, 11, January, 1970.

(22) Engin, A. E., "Axisymmetric response of a fluid-filled spherical shell to a local radial impulse - a model for head injury", J. of Biomechanics, Vol. 2, No. 3, 325, July, 1969.

(23) Liu, Y. King and Nelson III, J. A., "Intracranial pressure wave propagation in head impact," submitted to J. Neurosurg. for publication.

(24) Barton, A. C., Physiology and Biophysics of Circulation. Year Book Medical Publishers, Chicago, 1965.

(25) Lingren, S. O. "Experimental studies of mechanical effects in head injury" Acta Chirurgica Scandinavica, Supp. 360, 1966.

(26) Unterharnscheidt, F. and Sellier, K. "The mechanics of the impact of violence on the skull" Proc. 3rd Int'l. Cong. of Neuro. Surg., Copenhagan, August, 1965.

(27) Lee, Y. C. and Advani, S. H., "Forced axisymmetric response of a fluid-filled spherical shell", to appear in 5th Southeast Conf. on Theor. & Appl. Mech., 1970.

(28) Chan, H. S., pending Ph.D. dissertation, Tulane University, 1970.

(29) Holbourn, A. H. S., "Mechanics of head injury" Lancet, 11, p. 438, 1943.

(30) Engin, A. E. and Wang, H. C., "A mathematical model to determine

viscoelastic behavior of in vivo primate brain", J. of Biomechanics, 3, No. 3, 283, May, 1970.

(31) Ommaya, A. K., Hirsh, A. E., & Martinez, J., "The role of whiplash in cerebral concussion", Proc. Tenth Stapp Car Crash Conference, New York: Soc. Automotive Engineering, p. 197-203, 1966.

(32) Unterharnscheidt, F. & Higgins, L. S., "Pathomorphology of experimental head injury due to rotational accoleration" Acta Neuropathologica, Vol. 12, p. 200-204, 1969.

(33) Martinez, J. L. and Garcia, D., "A model for whiplash" J. of Biomechanics, 1, 23-32, 1968.

(34) Roberts, S. B., Ward, C. C. and Nahum, A. M., "Head trauma - a parametric dynamic study" J. of Biomechanics, 2, 397-415., 1969.

(35) Hayashi, T., "Brain shear theory of head injury due to rotational impact" to appear Jour. of the Faculty of Engineering, Univ. of Tokyo, 31, No. 2, September, 1970.

(36) Lee, Y. C. and Advani, S. H., "Transient response of a sphere to torsional loading -- a head injury model" Math. Biosciences, 6, 473-486, 1970.

(37) Holladay, A. and Bowen, I. G., "A mathematical model of the lung for studies of mechanical stress" Proc. of the San Diego Symp. for Biomed. Engr., 39-50, 1963.

24

ACKNOWLEDGEMENTS

This paper was written while the author was partially supported by grants No. EC 00402-04 and EC-00087-03 from the National Institute of Environmental Health Service of the U. S. Public Health Service and Contract No. F 33615-70-C-1565 from the Aerospace Medical Research Lab., U. S. Air Force Systems Command.

LIST OF FIGURES

Figure 18. Pressure distribution at the time of intermediate coup. Note the sharply-focused area at grades 5, 4, 3 and 2.

Figure 19. Cumulative Damage Criterion for a closed head injury. The damage mechanism is proportional to the averaged time spent at a given location beyond a critical negative pressure, p*.

Figure 20. Locations of cumulative brain damage for a time-varying polar-cap load. The most likely location is grade 5, and the least is grade +. The rest of the grades are linearly scaled. Note the absence of contrecoup.

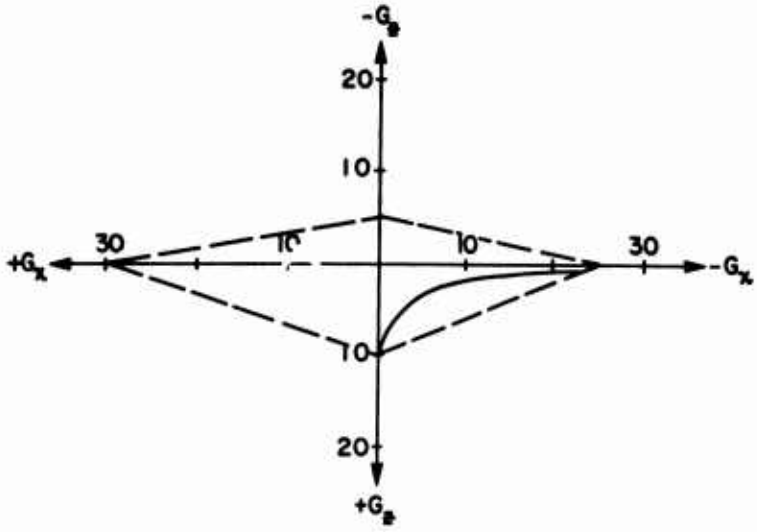

Figure 1. Possible injury tolerance curves for the G_x-G_z plane.

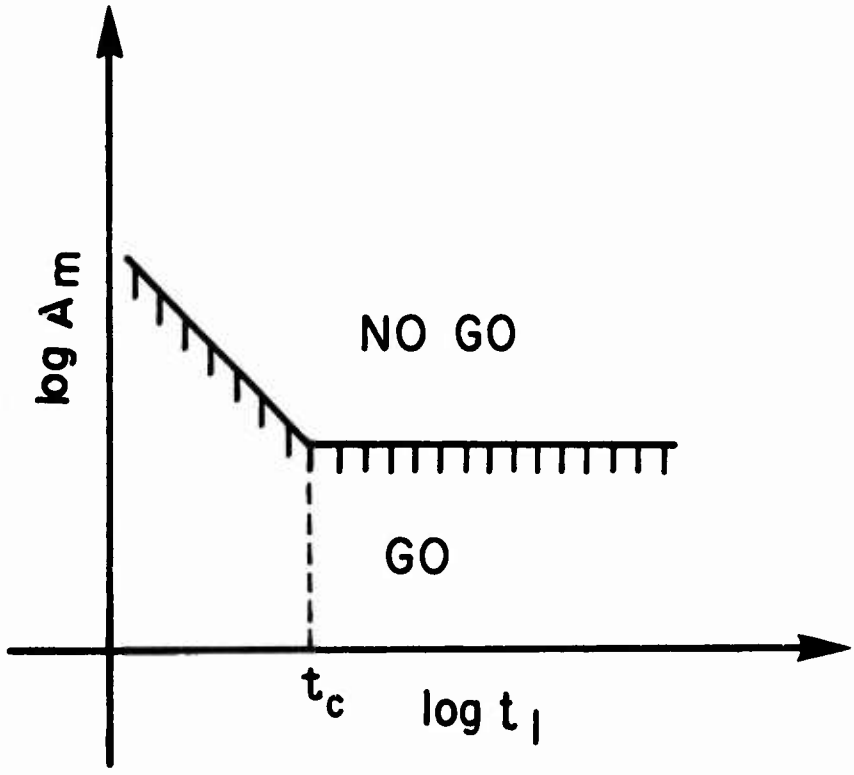

Figure 2. Typical tolerance graph based on equal tissue strain assumption. A_m and t_1 are the peak acceleration and duration of the applied pulse respectively. t_c is the critical pulse duration.

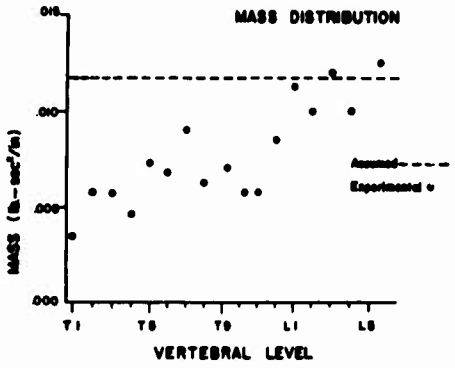

Figure 3. Mass distribution of the humar cadaver trunk. Dotted line is data assumed in Ref. 9.

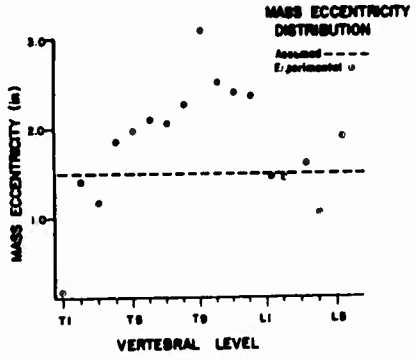

Figure 4. Mass eccentricity distribution of the human cadaver trunk. Dotted line is data assumed in Ref. 9.

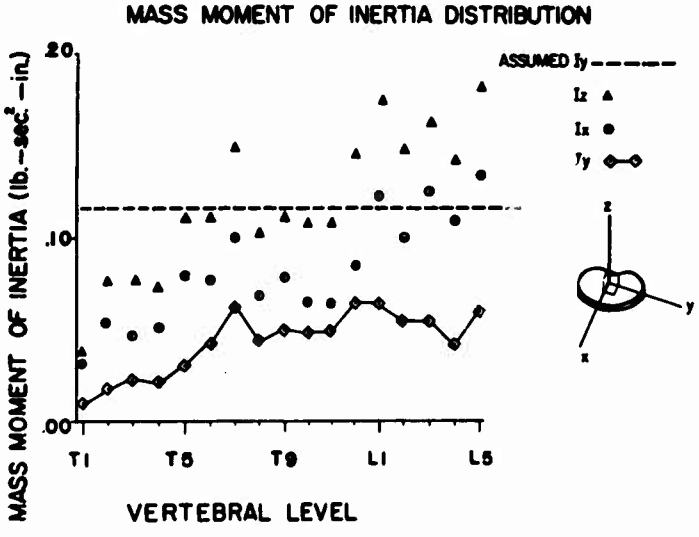

Figure 5. Mass moments of inertia distribution of the human cadaver trunk. Dotted line is data assumed in Ref. 9.

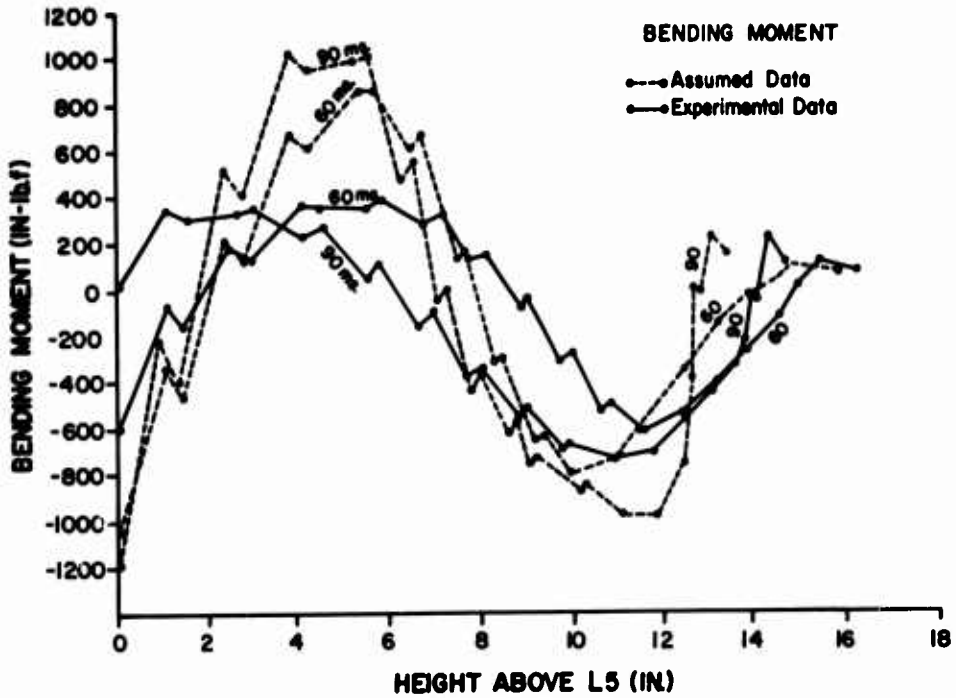

Figure 6. Moment distribution along the spine due to a 10g caudocephalad ($+G_z$) acceleration pulse at 60 and 90 milliseconds. Dotted lines denote result using the data assumed in Ref. 9.

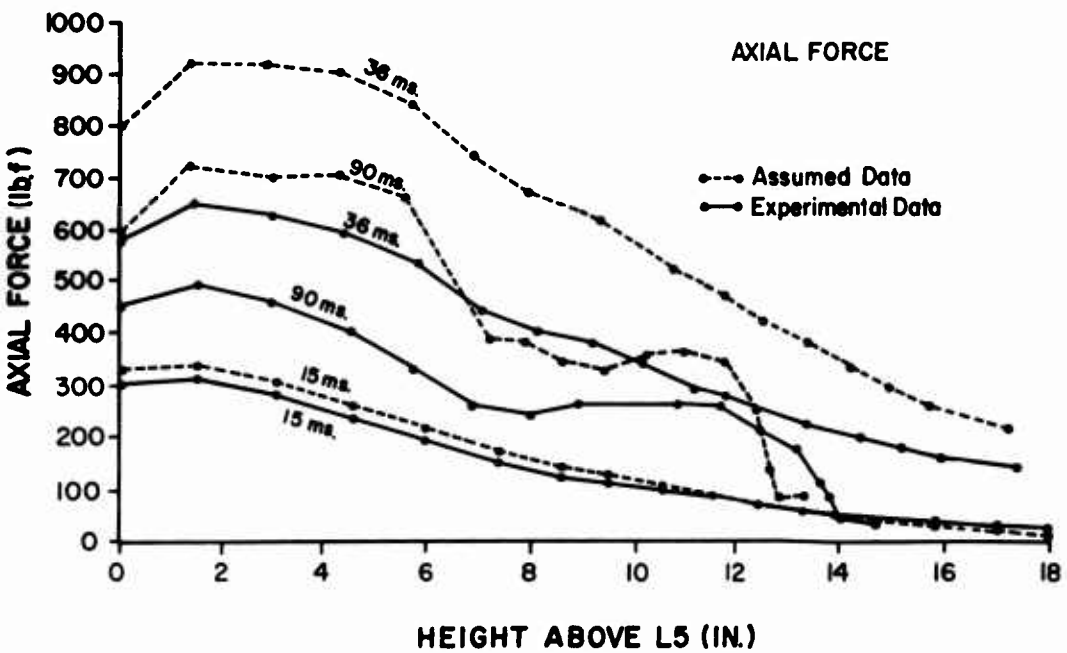

Figure 7. Axial force distribution along the spine due to a 10g caudocephalad ($+G_z$) acceleration pulse for different times. Dotted lines denote result using data assumed in Ref. 9.

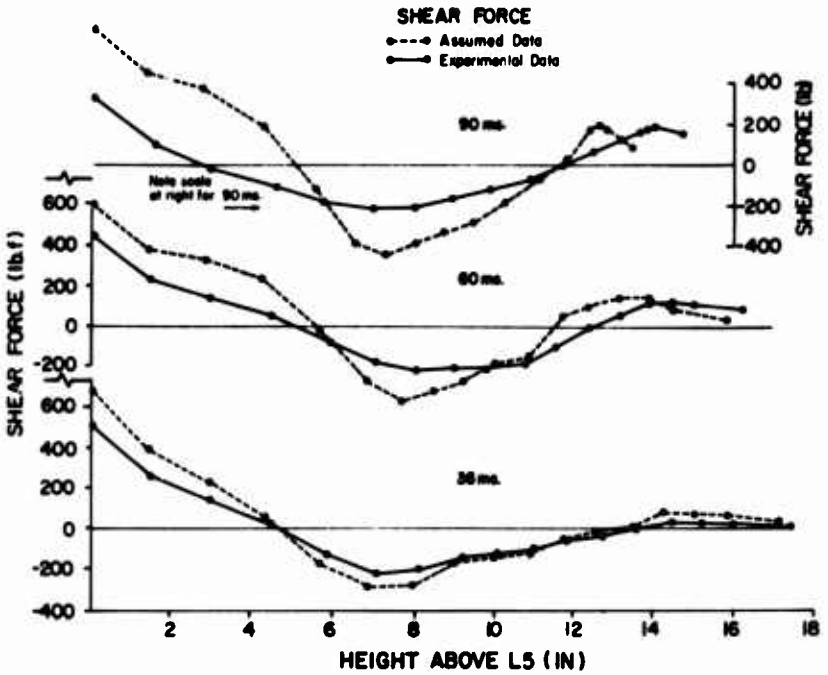

Figure 8. Shear force distribution along the spine due to a 10g caudocephalad ($+G_z$) acceleration pulse for different times. Dotted lines denote result using data assumed in Ref. 9.

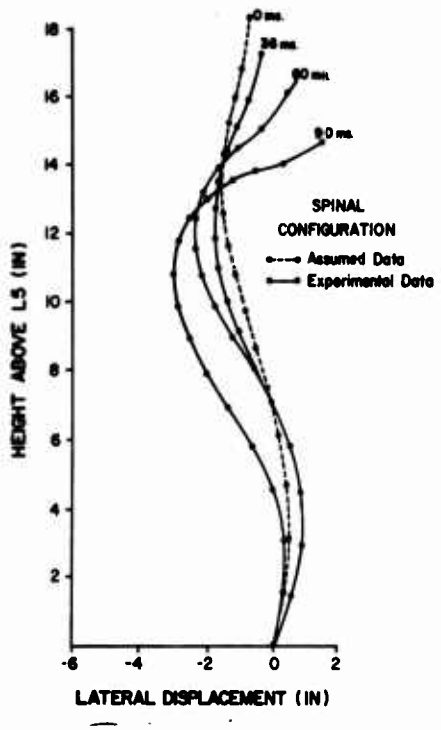

Figure 9. Time-history of configuration changes of the spine.

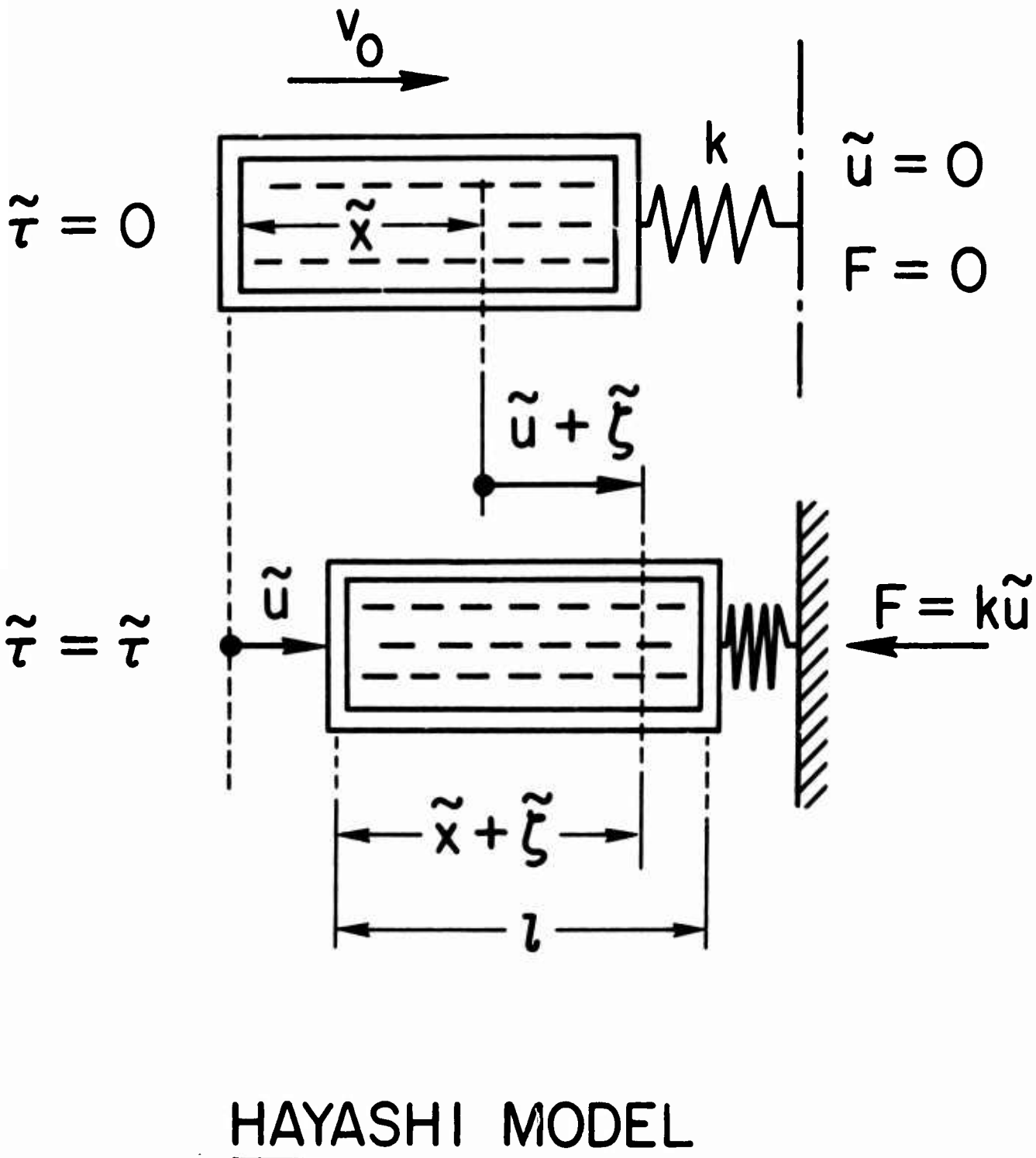

Figure 10. One-dimensional continuum model of head injury by Hayashi[14].

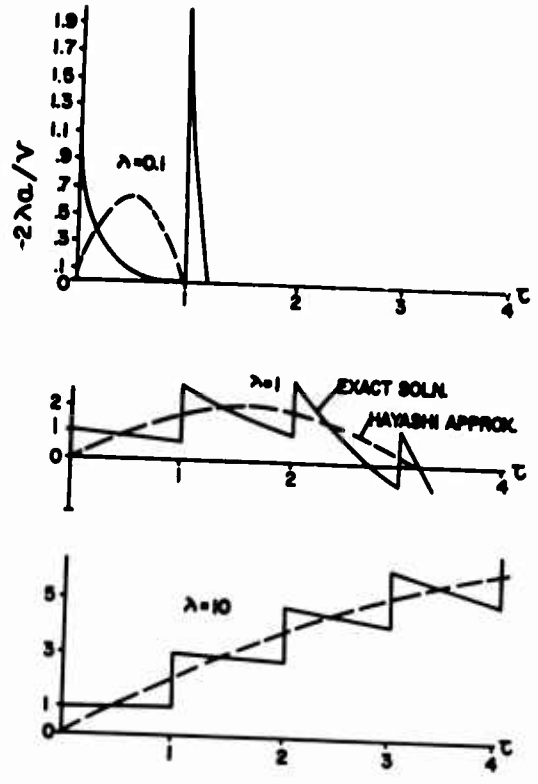

Figure 11

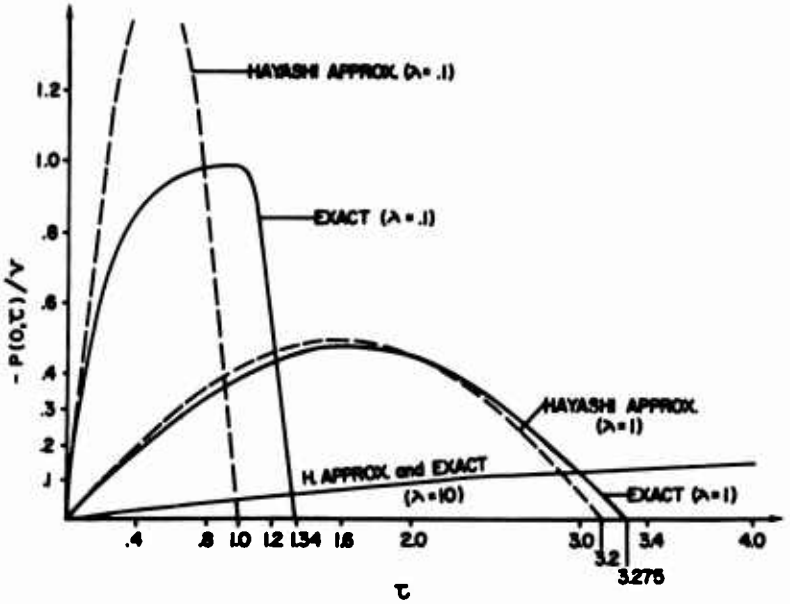

Figure 12

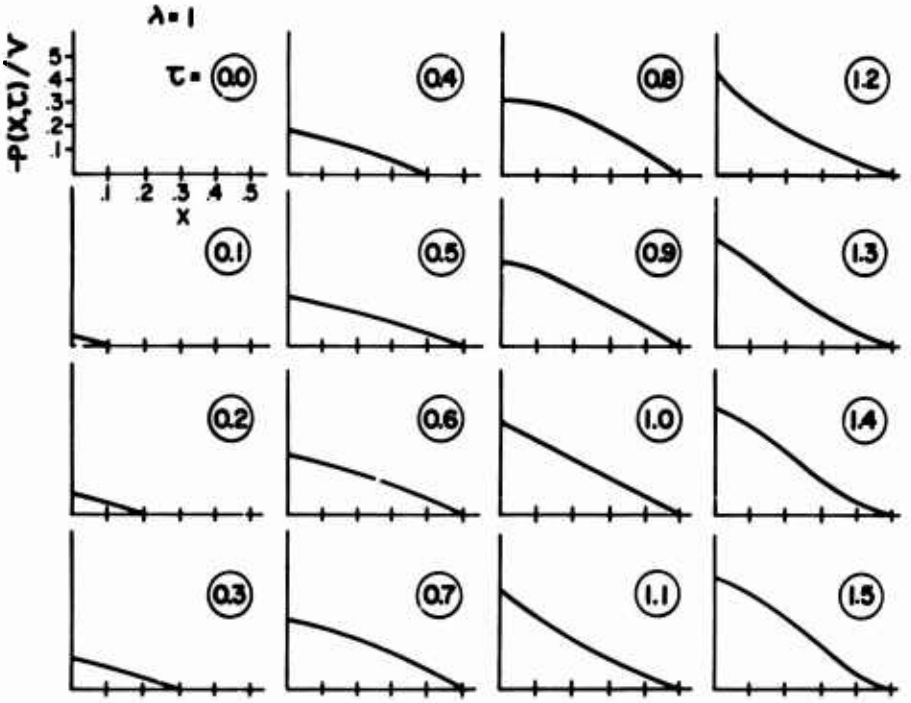

Figure 13

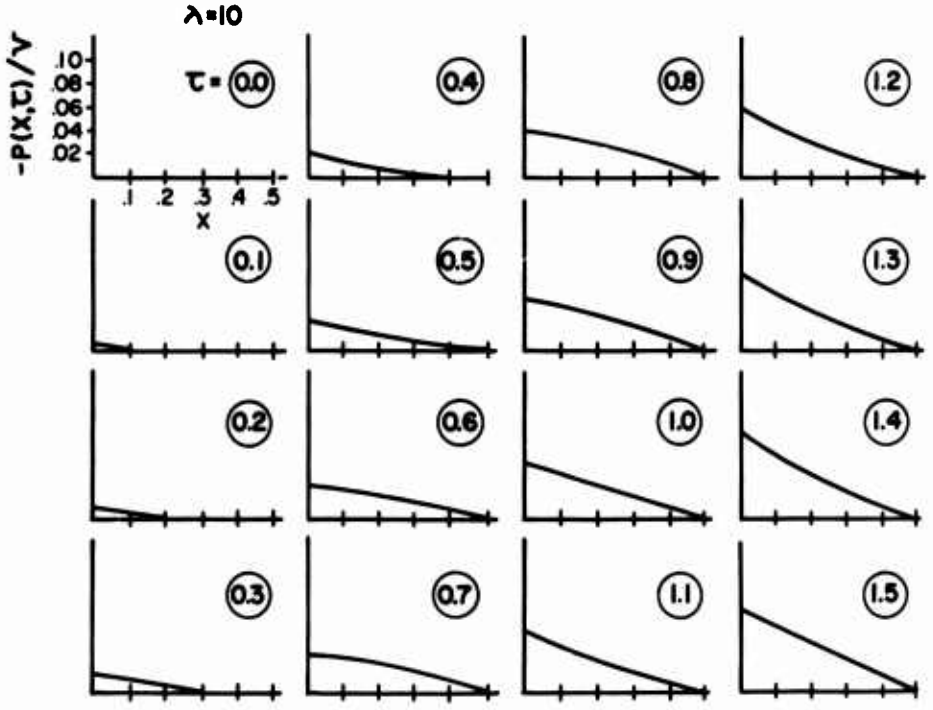

Figure 14

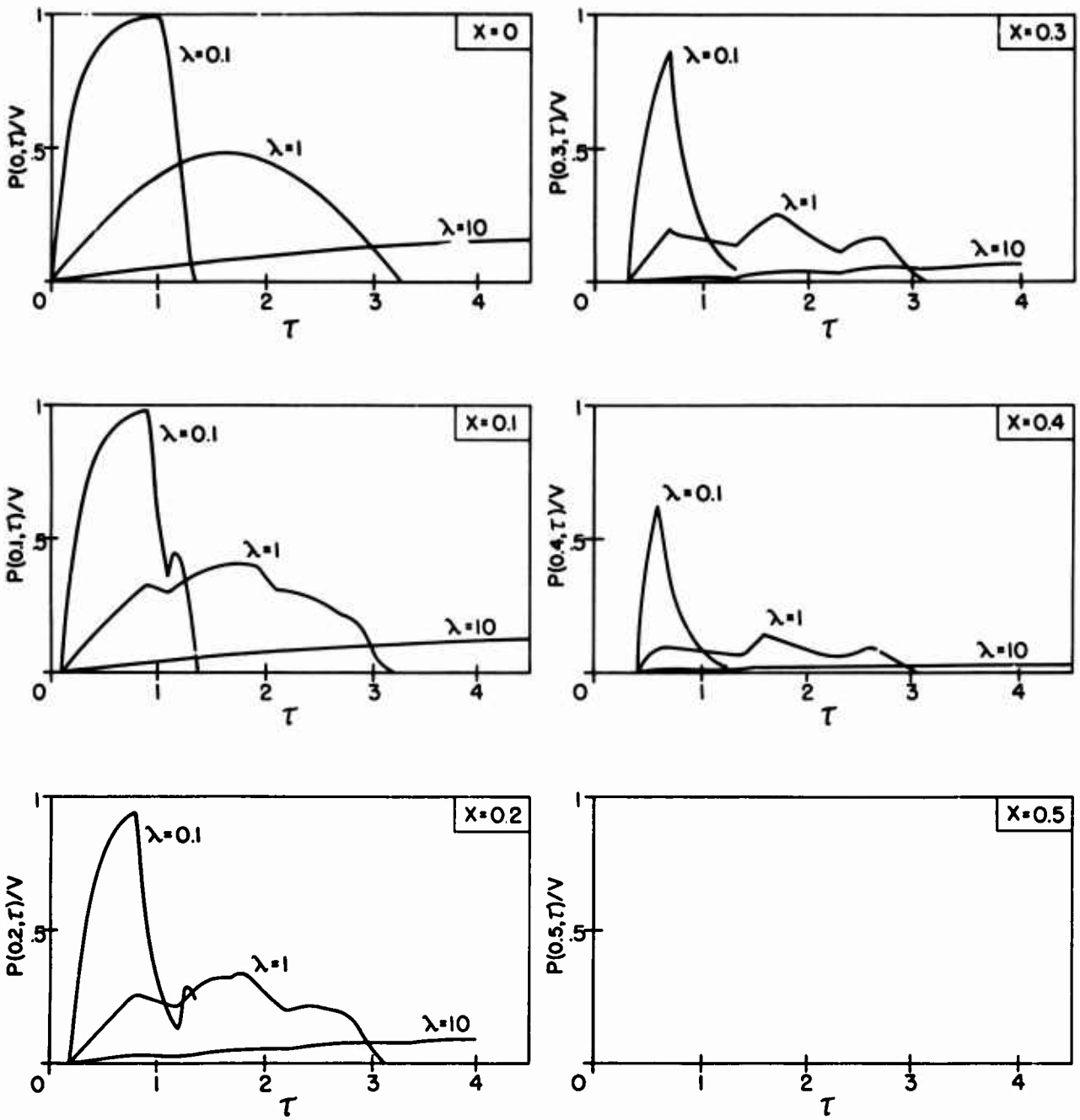
X=0
λ=0.1
λ=1
λ=10
P(0,τ)/V
X=0.3
P(0.3,τ)/V
X=0.1
P(0.1,τ)/V
X=0.4
P(0.4,τ)/V
X=0.2
P(0.2,τ)/V
X=0.5
P(0.5,τ)/V
τ

Figure 15

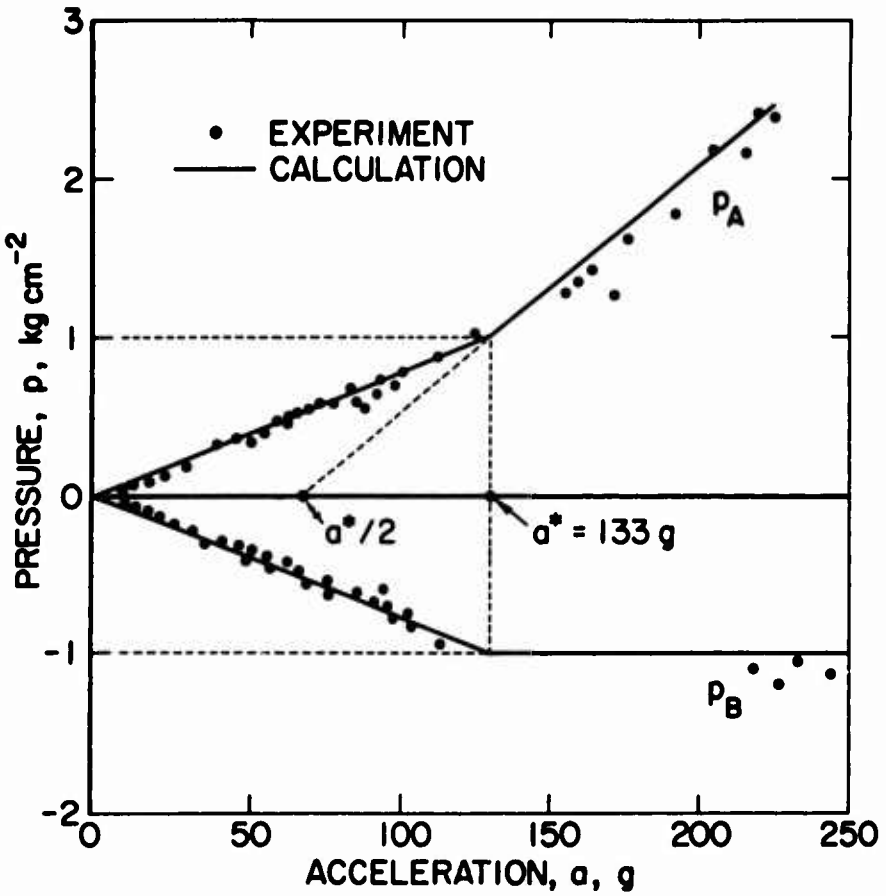

Figure 16. Comparison of theory with experiment according to Hayashi. P_A=pressure at coup; P_B=pressure at contrecoup.

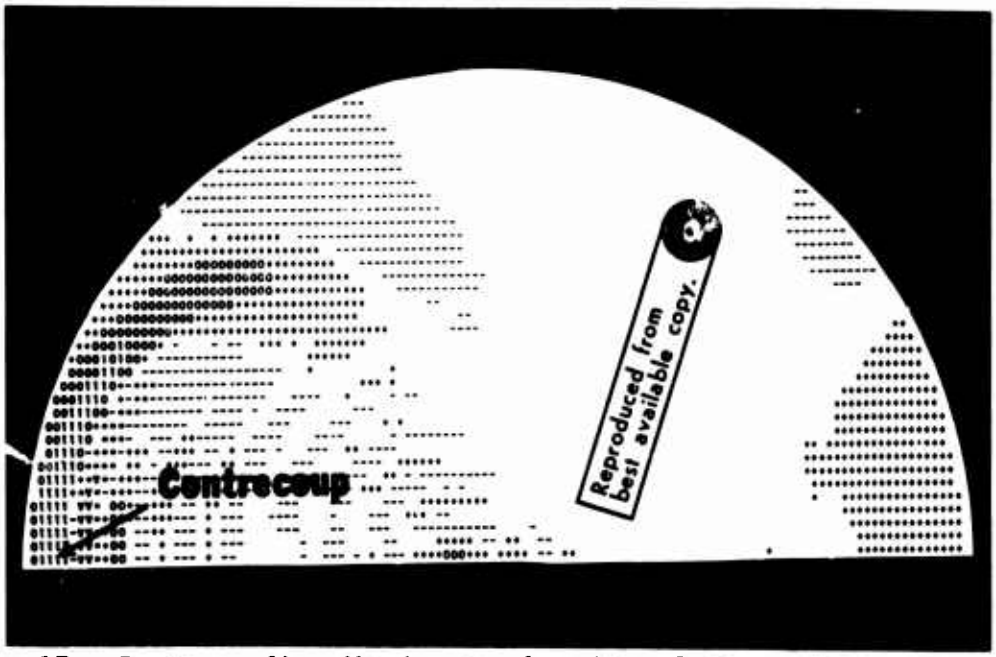

Figure 17. Pressure distribution at the time of approximate contrecoup. Note the relatively large diffuse area at grade 1.

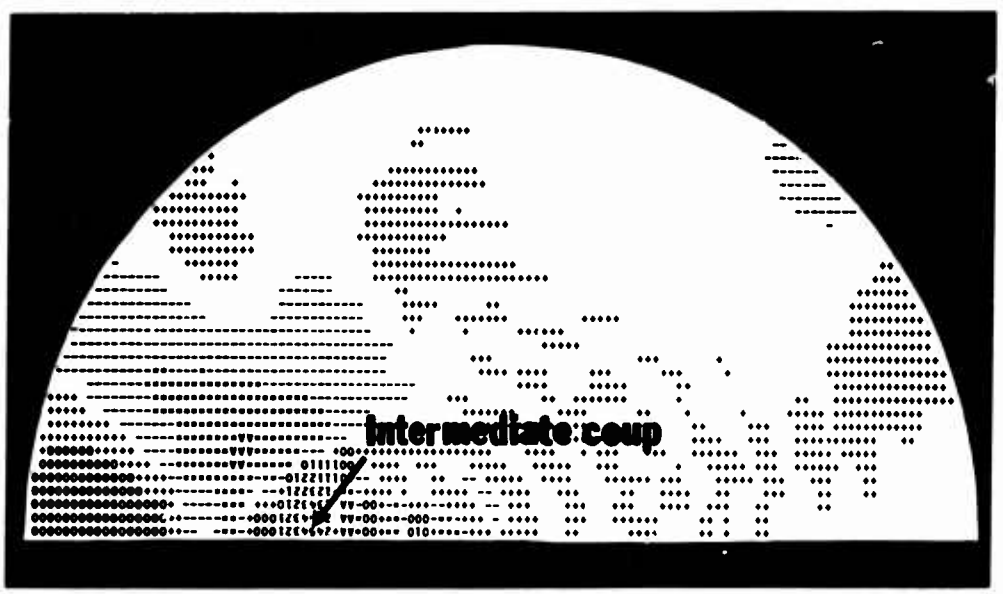

Figure 18. Pressure distribution at the time of intermediate coup. Note the sharply-focused area at grades 5, 4, 3 and 2.

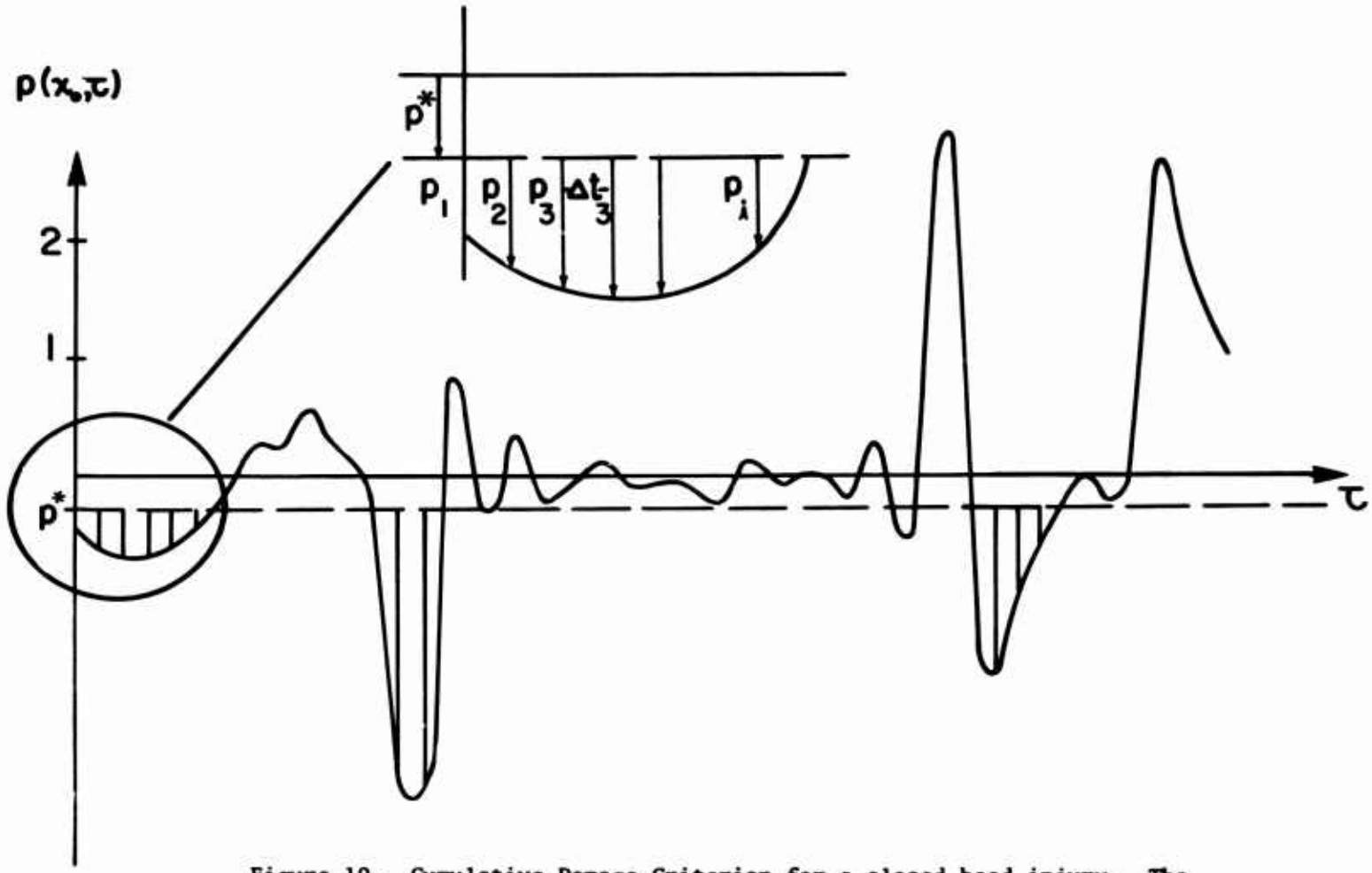

Figure 19. Cumulative Damage Criterion for a closed head injury. The damage mechanism is proportional to the averaged time spent at a given location beyond a critical negative pressure, p*.